



LAWRENCE  
LIVERMORE  
NATIONAL  
LABORATORY

# $N = 3 - 3$ Transitions of Ne-like Ions in the Iron Group, Especially Ca(10+) and Ti(12+)

Y. Ishikawa, J. Lopez Encarnacion, E. Träbert

October 10, 2008

Physica Scripta

## **Disclaimer**

---

This document was prepared as an account of work sponsored by an agency of the United States government. Neither the United States government nor Lawrence Livermore National Security, LLC, nor any of their employees makes any warranty, expressed or implied, or assumes any legal liability or responsibility for the accuracy, completeness, or usefulness of any information, apparatus, product, or process disclosed, or represents that its use would not infringe privately owned rights. Reference herein to any specific commercial product, process, or service by trade name, trademark, manufacturer, or otherwise does not necessarily constitute or imply its endorsement, recommendation, or favoring by the United States government or Lawrence Livermore National Security, LLC. The views and opinions of authors expressed herein do not necessarily state or reflect those of the United States government or Lawrence Livermore National Security, LLC, and shall not be used for advertising or product endorsement purposes.

# $N = 3 - 3$ transitions of Ne-like ions in the iron group, especially $\text{Ca}^{10+}$ and $\text{Ti}^{12+}$

Yasuyuki Ishikawa<sup>1</sup>, Juan López Encarnación<sup>1</sup> and Elmar Träbert<sup>2,3</sup>

<sup>1</sup> Department of Chemistry and the Chemical Physics Program, University of Puerto Rico, P. O. Box 23346, San Juan, Puerto Rico 00931-3346, USA

<sup>2</sup> Astronomisches Institut, Ruhr-Universität Bochum, D-44780 Bochum, Germany

<sup>3</sup> High Temperature and Astrophysics Division, LLNL, P.O. Box 808, Livermore, CA 94551, USA

E-mail: traebert@astro.rub.de

## Abstract.

The Ti XIII  $2s^22p^53l - 3l'$  and  $2s2p^63l - 3l'$  transitions that have been discussed previously on the basis of beam-foil spectra and laser-produced plasmas in comparison to semi-empirically scaled computations have now been treated by accurate *ab initio* Multi-reference Møller-Plesset calculations. While most  $2s^22p^53l - 3l'$  line identifications are supported by the new calculations, the  $2s2p^63l - 3l'$  transition arrays are revised. Theoretical level positions are given for all elements from Ca through Fe. The quality of the calculation is demonstrated on beam-foil spectra of Ca.

PACS numbers: 3230Jc, 3115am, 3450Fa

Submitted to: *Phys. Scr.*

## 1. Introduction

Ne-like ions with their closed shell ground configuration figure prominently in the charge state distributions of many plasmas. They have also been the basis of some of the first EUV laser schemes (then called x-ray lasers) [1], although the actual lasing lines seemed to be different from what had been expected. This surprise was later resolved when the understanding of the laser-produced plasmas that provided the lasing medium improved [2, 3]. Ne-like ion lines in the x-ray regime have been studied with high accuracy at tokamak plasmas in Princeton [4], and strong x-ray lines of Ne-like heavy ions are being discussed for plasma diagnostics of the ITER tokamak fusion reactor project. Last, but not least, the interpretation of Ne-like x-ray spectra of Fe and Ni has been fought over when solar and laboratory data (mostly from electron beam ion traps (EBIT)) scattered much and seemed to be inconsistent [5]. Some of the problems appear to have rooted in insufficient control over experimental conditions, and the recent results have converged

towards the Livermore EBIT data set. At the same time, some of the theoretical approaches appear to have been advertised beyond their actual applicabilities; after several rounds of corrections, some, but not all of the calculational inconsistencies have been reduced.

We are involved in an effort to validate theoretical assumptions, approximations and procedures for such cases, including Ne-like ions, in comparison to extreme ultraviolet (EUV) and soft-x-ray spectra. We have therefore applied our relativistic state-specific multireference Møller-Plesset perturbation theory formalism [6, 7, 8] to the  $2s^22p^53l$  and  $2s2p^63l$  levels of Ne-like ions of iron group elements. For the transitions between these levels, extensive observations of laser-produced plasmas [9] and foil-excited ions beams [10, 11] (especially of Ti) are available that so far have been compared only with semiempirically scaled calculations. There also are solar observations (mostly of Fe), continuing with the most recent *Hinode* spacecraft, that we will address elsewhere.

Most of the previous analyses of the spectrum Ti XIII concern  $2s^22p^53l - 3l'$  transitions, and little ambiguity remains for those. These levels are well suited for an isoelectronic comparison to the results of various calculations [12]. In addition, systematic lifetime measurements in Ti XIII [13] have supported the line identifications, even as some scatter of the theoretical lifetime pattern persists [14]. The situation is quite different for the  $2s2p^63l$  levels. An early attempt at assigning lines to the  $2s2p^63l - 3l'$  transitions on the basis of beam-foil spectra [15] was undertaken with the very limited theoretical guidance available at the time [16, 17, 18], and the results have to be revised.

Later attempts at localizing  $2s2p^63l$  levels by their decays to  $2s^22p^53l$  levels suffered from line blends and from computational problems with severe level mixing [21, 22]. Here we suggest new line identifications in the old spectra, which are consistent with our calculations. At the same time we find that along the isoelectronic sequence some levels are calculated by our algorithms in positions systematically (slightly) different from the experimental analysis.

Of course, the  $n=3$  levels are not the only ones of interest. For example, the analysis up to  $n=4$  levels has been demonstrated in [23].

## 2. Computational method and results

We recently have developed a version of a relativistic state-specific multireference Møller-Plesset (MR-MP) perturbation theory [6, 7, 8] based on a state-averaged multiconfiguration Dirac-Fock-Breit self-consistent-field (MCDFB SCF) and multireference configuration interaction (MR-CI) procedures [24]. This approach has been very successful in identifying lines in the spectra of ions of a variety of isoelectronic sequences.

The starting point is the state-averaged MCDFB SCF calculation to define a common set of spinors for all the states included in the state-averaged MCDFB SCF and subsequent MR-CI. The state-averaged MCDFB SCF for the ground and low-lying excited  $J = 0 - 4$  states in the neon-like ions were carried out including 13 even- and 20

odd-parity configuration-state functions (CSFs) arising from the  $2s^22p^53l$  and  $2s2p^63p$  configurations. The single set of Dirac spinors provides, in finite-order perturbation theory, a well-balanced representation of dynamic correlation energy corrections on term energy separations. The large and small radial components of the Dirac spinors were expanded in sets of even-tempered 26s24p20d Gaussian-type functions that satisfy the boundary conditions associated with the finite nucleus [25]. The Gaussian exponents are geometrical series  $\gamma_i = \alpha\beta^{(i-1)}$ , where  $\alpha=0.5324$  and  $\beta=2.20$ . The speed of light was taken as 137.0359895 in all calculations.

The MR-CI includes a total of 37 CSFs arising from the  $2s^22p^53l$  and  $2s2p^63l$  configurations. The frequency-dependent Breit interaction, the Lamb shift, normal and specific mass shifts were evaluated as the first-order corrections using the MR-CI eigenvectors [7]. Subsequently, each of the 37 MR-CI eigenstates was subjected to state-specific MR-MP refinement to account for the residual dynamic correlation. The order of the partial-wave expansion, the highest angular momentum of the spinors included in the MR-MP perturbation theory calculations, is  $L = 11$  throughout this study.

### 3. Ti XIII

Among the multitude of Ne-like ions studied, Ti<sup>12+</sup> plays a special role because of the many observations of its EUV spectrum, much of the work using laser-produced plasmas or beam-foil spectroscopy (BFS). Both light sources operate at a rather high particle density (in the exciter foil of BFS, the density is that of a solid). Hence many levels can be populated, even those that require more than one step of excitation from the ground state. Because of this, not only the  $2p^53s$ ,  $2p^53d$ , and  $2s2p^63p$   $J = 1$  resonance levels and those levels that are subsequently reached along their decay chains are populated, but also levels in configurations such as  $2p^53p$  and  $2s2p^63d$ , with any value of  $J$ . Especially the  $2s2p^63d$  levels come close to those of other configurations, and mixing effects affect the level positions, rendering predictions less reliable. Predictions, however, are much needed, because these non-resonance levels are hardly excited in classical light sources, and spectroscopic reference data are sparse. Our results on Ti XIII are listed in table 1, together with data from the NIST data base [26].

It is no surprise that the  $2p^53l$  levels are better known than most of the  $2s2p^63l$  levels. In fact, in a series of publications, the atomic spectroscopy groups at Lund and Bochum have converged in their analyses for the  $2p^53l$  levels [22]. Yrast level multiplets (levels of maximum angular momentum  $\ell$  for a given principal quantum number  $n$ , here for  $n > 4$ ) were measured at Bochum and analyzed at Lund, and it was attempted (with limited success) to identify lines that would put more of the core-excited  $2s2p^6nl$  levels on an absolute footing [20]. Indeed, two lines near 121 Å were identified as likely candidates for  $2s2p^63l$  level decays in Ti XIII (and corresponding lines in the spectra of Sc XII and V XIV). In a way, one blind spot remained, the transitions between  $2s2p^63l$  levels. Träbert [10] had tried to identify these lines in the Bochum beam-foil spectra of titanium, using trial and error guided by the very few calculations that were available

at the time. The basis of this analysis is illustrated in [15], where the very different predictions are plotted. In hindsight, the calculation by Crance [16] had a  $2p^5 3s \ ^3P_{1,2}$  level splitting that was too large (while the HXR calculations by Fawcett [18, 19] gave a difference that was too small), and the  $2p^5 3p \ ^1S_0$  level was predicted at a position more than  $2000 \text{ cm}^{-1}$  too high. Among the  $2s2p^6 3l$  levels, Fawcett's predictions were  $1000$  to  $2000 \text{ cm}^{-1}$  high whereas the  $2s2p^6 3s$  levels given by Bureeva and Safronova [17] were some  $3000 \text{ cm}^{-1}$  low. The latter's  $2s2p^6 3d$  levels were not all just shifted by the same amount: the  $^3D_J$  levels were about  $2000 \text{ cm}^{-1}$  high, and the  $^1D_2$  level was almost  $10000 \text{ cm}^{-1}$  too low. In brief, some of the calculations yielded a decent pattern of level positions, but at an overall misleading mean energy; another was much better for the mean energy, but poorer for the level spacings, and so on. Christer Jupén later informed Träbert that those experimental levels in [15] were wrong, but he could not offer a consistent data set to replace them. Perhaps amusingly, this faulty set of level values was adopted for the NIST online data base, being the only such set of level values for the  $2s2p^6 3l$  levels of any Ne-like ion. Again in hindsight (and corroborated by the present calculations), those  $2s2p^6 3d \ ^3D_J$  level values turned out as too low by almost  $2000 \text{ cm}^{-1}$ , and the  $^1D_2$  level was some  $20000 \text{ cm}^{-1}$  too low. Two of the  $2s2p^6 3p$  levels connect by E1 transitions to the ground state and have therefore been known (with moderate accuracy) for quite some time; the  $2s2p^6 3p$  level values scatter around the newly calculated level positions by some  $300 \text{ cm}^{-1}$ . This scatter corresponds to about three line widths (FWHM) in the better resolved of the Bochum beam-foil spectra of Ti. An *ab initio* calculation with such accuracy is remarkable.

Our new calculations offer a fresh view at the the  $2s2p^6 3l$  level problem. We have checked the newly predicted line positions (tables 2, 3) against the old beam-foil spectra (still the best source of information on the excitation of core-excited ions), and find no significant disagreement of the predicted spectrum with the structures observed. Because of additional decay branches to lower configurations, the  $2s2p^6 3l - 3l'$  lines are generally much weaker than the corresponding  $2p^5 3l - 3l'$  transitions in the same spectral range. We have therefore listed the computed branch fraction along with the wavelengths. In addition, and very much dependent on the conditions of the light source, there is the excitation process that is bound to put less population into higher lying levels. For a detailed analysis, it would be good to have a collisional-radiative model that involves excitation processes and radiative rates, so that realistic relative line intensities can serve as an additional tool in the spectral analysis. This we do not have at our disposal; moreover, many of the relatively weak lines are close to lines from other spectra of Ti.

The highest of the  $2s2p^6 3d$  levels,  $^1D_2$ , features several decay branches in the  $117$  to  $134 \text{ \AA}$  range, neither of which thus is prominent. The most meaningful branch would be to the  $2s2p^6 3p \ ^1P_1^o$  level, near  $362 \text{ \AA}$ , where it is probably blended with several other lines [10]. The  $2s^2 2p^5 3d$  levels have weak decay branches to  $2s2p^6 3p \ ^3P_J^o$  levels (wavelengths about  $360 - 380 \text{ \AA}$ ), but the dominant decays are expected near  $121 \text{ \AA}$ , where Jupén *et al* [20] have noted two spectral lines (and some higher spectral background nearby) as

likely signatures of such transitions. Although a rather weak branch (13%), the  $2s2p^63d\ ^3D_3$  level decay to the  $2s2p^63p\ ^3P_2$  level, predicted at 381.34 Å, may be identified with a suitably weak line at 381.6 Å. The weaker components of the predicted multiplet are close to spectral structures that are too weak to quantify a reliable line position. Among the four  $2s2p^63p$  levels, the two  $J = 1$  levels decay predominantly to ground (near 21 Å); Träbert [10], however, taking the branching fractions into account, has suggested candidate lines for the  $2s2p^63s\ ^3S_1 - 2s2p^63p\ ^3P_J^o$  line multiplet in which the strongest component is blended with another, similarly intense line. On these three lines hinges the experimental level position of the  $2s2p^63s\ ^3S_1$  level which disagrees with our calculation by about  $1000\text{ cm}^{-1}$ . The line of interest falls in between several lines of the  $2p^53s - 2p^53p$  transition array which can be expected to be brighter (singly excited levels) and thus possibly hide the  $2s2p^63p$  level decays. If, for example, the  $2s2p^63s\ ^3S_1 - 2s2p^63p\ ^3P_2^o$  line was not at 474.45 Å [10], but blended with the  $2p^53s - 2p^53p$  transition at 472.09 Å [10], the mismatch of the  $2s2p^63s\ ^3S_1$  level value with our calculation would practically vanish. An alternative assignment could be with a line at 473.2 Å, but that would again imply a blend with a brighter line. The available data do not enable a positive assignment. The  $2s2p^63s\ ^3S_1$  level has decay channels to the ground state and to singly excited levels, in the 120/121 Å and 127 Å ranges, where no positive identification has been possible yet. The neighbouring  $2s2p^63s\ ^1S_0$  level is poorly populated (low statistical weight) directly; the most likely cascade levels,  $2s2p^63p\ J = 1$ , decay predominantly to ground. For this reason no transition into the  $^1S_0$  level has been determined with confidence, nor any of the competing decays to singly excited  $3s$  levels (116 Å, 123 Å).

Without any better evidence than those 20 years old beam-foil spectra, one might see the spectral classification as being stuck. However, our new *ab initio* calculation is close to the level values of the  $2s2p^63p\ J = 1$  levels and makes predictions about  $2s2p^63d$  level decays that are compatible with the beam-foil spectra. The calculation thus appears about as reliable for  $2s2p^63l$  levels as for the  $2s^22p^53l$  levels. In the Bochum beam-foil spectra, the  $2s^22p^53l - 3l'$  lines are within 0.2 Å (better than 0.05% for the difference of level energies) of the calculated positions, with the single exception of the  $2s^22p^53s\ ^3P_2^o - 2s^22p^53p\ ^3S_1$  line near 551.5 Å, for which the wavelength mismatch reaches 0.6 Å or 0.1%. The beam-foil spectra do not contradict the predictions of transitions  $2s2p^63s - 3p - 3d$  thus possible, and therefore we argue in favour of adopting the new theoretical description of the  $2s2p^6nl$  levels.

#### 4. Isoelectronic sequence

We have applied the same calculation to Ne-like ions of elements from Ca ( $Z=20$ ) through Fe ( $Z=26$ ) (tables 4 - 9). (The results for Fe will be discussed elsewhere in comparison to recent astrophysical observations.) Our calculated level values agree closely with the NIST data tables (where only the  $2p^53l$  levels are listed), with minor exceptions: While for most levels the deviations between reference data and the results of our *ab initio*

calculations are about 0.01%, they are significantly larger (0.04%) for the  $2s^22p^53p\ ^1S_0$  levels. Such an effect has not been seen in other atomic systems, and the question arises whether the slight mismatch is caused by the calculation or by a problem of spectral data analysis. For example, we note that the  $2s2p^63p\ ^1S_0$  level has been hard to find [11] and was then disputed together with other (rather stronger) lines (involving the  $^3S_1$  level) [14]. Indeed, in Ti XIII, one of the two decay branches of the  $2p^53p\ ^1S_0$  level is blended with another line, and the line identification was supported by the similarity of the time constant of one of the decay curve components with that of the other candidate line [11]. There are other, even weaker lines nearby - too weak, in fact, to obtain sufficient signal for a meaningful decay curve analysis. In principle, we cannot rule out that the lines should be reidentified, but we have no better candidates. Only a collisional-radiative model might provide additional insight into the relative line intensities and thus provide another tool for spectral analysis.

Besides the comparison of calculated and measured values in a given spectrum, there is the option of isoelectronic sequence analysis. In the present case, the  $2p^53p\ ^1S_0$  level decay has been assigned in all elements across the iron group, finding a smooth isoelectronic trend in comparison to a semiempirically adjusted Hartree-XR calculation (see [11]); the relative energy offset to our calculation is rather constant. For a reassignment, alternative lines would have to be found in all those spectra; it is possible that such lines can be found among the very weak lines, but those cannot be analyzed reliably. Alternatively, the experimental record may be taken to be correct - which leaves us with the indication of a slight flaw in the otherwise excellent performance of our code package.

Tables 1 and 4 - 9 reveal several individual cases in which the differences between the NIST data base entries and our calculations exceed 0.1%. Such isolated discrepancies suggest problems with the original line identification.

We see the same good overall agreement of our results with the results obtained by Hibbert *et al* [12] ( $2p^53l$  levels only) and with the available spectroscopic data on Ne-like ions. Unfortunately, there are no high-quality beam-foil EUV survey spectra available as there are for Ti. The beam energy of the Bochum accelerator would not be sufficient to produce Ne-like ions in quantity much beyond Ti. For the neighbouring elements, Sc (Z=21), V (Z=23), and Cr (Z=24), (unevaluated) partial survey spectra are available (on request to ET).

## 5. Discussion and conclusions

The experimental coverage of Ne-like ions of the iron group concerns mostly  $2s^22p^53l$  levels, and because of the higher solar abundances, even-Z elements. The coverage is almost complete for elements above Z=20 (Ca), but not necessarily consistent. An *ab initio* calculation has the advantage of not being limited - as experiment is - by wavelength ranges, spectrometers, detectors, or observation conditions. However, for the most time, *ab initio* calculations of many-electron systems have not been accurate

enough for spectral analysis. Our application of modern calculations to the Ne-like ions of iron group elements demonstrate how well good predictions agree with the results of extensive experimental work. In fact, it should now be straightforward in many cases to identify lines on the basis of such predictions. We demonstrate this capability for the example of Ca.

The experimental data to compare with are beam-foil EUV spectra recorded at Bochum at ion beam energies of 8 and 11 MeV [27]. At these energies, the charge state distribution favours Ca<sup>9+</sup> (Ca X) and Ca<sup>8+</sup> (Ca IX), but the spectra contain prominent lines of the adjacent charge state ions as well. An R=2 m grazing incidence monochromator with a channeltron detector served as the dispersive element and selector. This instrument has an optimum detection efficiency near 200 Å [28, 29]; in the wavelength range of interest for the 3-3 transitions in Ca X, 350 to 900 Å, the detection efficiency is a factor of two to ten lower than the optimum. The actual Ca spectra recorded did not reach beyond about 600 Å and thus cover only part of the range of present interest. Between 425 and 475 Å, three individual spectra showed very reproducible line positions; the adjacent range up to 600 Å was only covered in a single spectrum. The wavelength calibration rests on the spectrometer mechanism supported by a micrometer-precision length gauge; the wavelength scale was tied to the 3s – 3p transitions in Ca X. The resonance line wavelength of Ca IX was reproduced to within 0.1 Å on this scale. Because of the narrow spacing of the few reference line wavelengths and their localization, we adopt this calibration scale uncertainty as the wavelength error, while the data statistics would permit to pinpoint each line with a higher precision onto the scale itself.

Table 10 shows the results: Practically all transitions with a predicted branch fraction higher than 10% can be associated with a spectral line of sensible intensity nearby, in most cases within 0.2 Å, and without a choice of many lines. (There are many more lines, but they are not so many as to make this a meaningless guessing game.) Some lines predicted as weak (by the branch fraction) show reasonably well, whereas the only line with a large branch fraction value (0.81) is from an upper level of  $J = 0$  which is expected to be weakly populated. The wavelength pattern consistency is remarkable. For many practical purposes, the calculated level values for Ca XI given in table 4 fill the wide gaps in the NIST data tables for this spectrum.

At this high level of computational accuracy, the process of line assignment changes from a tedious multi-step exercise of trial and error, assumption and refinement to one of largely instantaneous line identification and much faster convergence of level values. The presently displayed beam-foil data are not accurate enough to serve as a base for a definite term table, but possibly solar coronal data can now be identified for the purpose.

## Acknowledgments

ET acknowledges travel support from the German Research Association (DFG). Part of this work has been performed at LLNL under the auspices of the USDoE under contract

No. DE-AC52-07NA27344. YI acknowledges partial support from LLNL subcontract No. B568401.

## References

- [1] Matthews D L, Hagelstein P L, Rosen M D, Eckart M J, Ceglio N M, Hazi A U, Medecker H, MacGowan B J, Trebes J E, Whitten B L, Campbell E M, Hatcher C W, Hawryluk A M, Kauffman R L, Pleasance L D, Rambach G, Scofield J H, Stone G, and Weaver T A 1985 *Phys. Rev. Lett.* **54** 110
- [2] Nilsen J, Koch J A, Scofield J H, MacGowan B J, Moreno J C and Da Silva L B 1993 *Phys. Rev. Lett.* **70** 3713
- [3] Li Y, Pretzler G and Fill E E 1995 *Phys. Rev. A* **52** R3433
- [4] Beiersdorfer P, von Goeler S, Bitter M, Hinnov E, Bell R, Bernabei S, Felt J, Hill K W, Hulse R, Stevens J, Suckewer S, Timberlake J, Wouters A, Chen M H, Scofield J H, Dietrich D D, Gerassimenko M, Silver E, Walling R S, and Hagelstein P L 1988 *Phys. Rev. A* **37** 4153
- [5] Brown G V 2008 *Can. J. Phys.* **86** 199
- [6] Vilkas M J and Ishikawa Y 2003 *Phys. Rev. A* **68** 012503
- [7] Vilkas M J and Ishikawa Y 2005 *Phys. Rev. A* **72** 032512
- [8] Vilkas M J, Ishikawa Y and Träbert E 2006 *J. Phys. B: At. Mol. Opt. Phys.* **39** 2195
- [9] Litzén U and Jupén C 1984 *Phys. Scr.* **30** 112
- [10] Träbert E 1984 *Z. Physik A* **319** 25
- [11] Träbert E and Jupén C 1987 *Phys. Scr.* **36** 586
- [12] Hibbert A, LeDourneuf M and Mohan M 1993 *Atomic Data Nucl. Data Tables* **53** 23
- [13] Träbert E 1986 *Z. Physik. D* **1** 283
- [14] Ivanova E P and Glushkov A V, *J. Quant. Spectrosc. Radiat. Transfer* 1986 **36** 127
- [15] Träbert E 1985 *Nucl. Instrum. Meth. B* **9** 626
- [16] Crance M 1973 *At. Data* **5** 183
- [17] Bureeva L A and Safronova U I 1979 *Phys. Scr.* **20** 81
- [18] Fawcett B C (private communication)
- [19] Cowan R D, *The theory of atomic structure and spectra*, University of California Press, Berkeley, 1981.
- [20] Jupén C, Litzén U, Träbert E 1996 *Phys. Lett. A* **214** 273
- [21] Jupén C, Litzén U, Träbert E 1996 *X-ray Lasers 1996 Conference, Inst. Phys. Conf. Ser. No 151: Section 11* 386
- [22] Jupén C, Litzén U, Träbert E 1996 *Phys. Scr.* **53** 139
- [23] Jupen C, Litzén U, Kaufman V and Sugar J 1987 *Phys. Rev. A* **35** 116
- [24] Vilkas M J, Ishikawa Y and Koc K 1998 *Phys. Rev. E* **58** 5096
- [25] Ishikawa Y, Koc K and Schwarz W H E 1997 *Chem. Phys.* **225** 239
- [26] Ralchenko Yu, Jou F-C, Kelleher D E, Kramida A E, Musgrove A, Reader J, Wiese W L and Olsen K 2005 *NIST Atomic Spectra Database (version 3.0.2)*, Online available at <http://physics.nist.gov/asd3>, National Institute of Standards and Technology, Gaithersburg, MD, USA
- [27] Träbert E, Pinnington E H, Kernahan J A, Doerfert J, Granzow J, Heckmann P H and Hutton R 1996 *J. Phys. B: At. Mol. Opt. Phys.* **29** 2647
- [28] Träbert E, Heckmann P H, Raith B and Sander U 1980 *Phys. Scr.* **22** 363
- [29] Träbert E 1984 *Phys. Scr. T* **8** 112

**Table 1.** Level energies of  $2s^22p^53l$  and  $2s2p^63l$  levels in Ti XIII. Comparison of the results of our calculations with NIST on-line data basis [26] and other experimental work. Deviations (in percent) are relative to our calculations. The  $LS$  term designations [10] are somewhat arbitrary for some mixed levels;  $jj$  labels are given, for example, in [22]. We supplement the  $LS$  terms by  $J(\#)\Pi$  with total angular momentum  $J$ , sequence number  $\#$ , and parity (\* for odd parity).

In- dex	Config- uration	Term $J(\#)\Pi$	Energy ( $cm^{-1}$ )						
			This work	NIST [26]	Dev.	[10]	Dev.	[22]	Dev.
1	$2s^22p^6$	$^1S\ 0(1)$	0	0	-	0	-	0	-
2	$2s^22p^53s$	$^3P^o\ 2(1)^*$	3697789	3698153	0.010	3698080	0.008	3698321	0.014
3		$^3P^o\ 1(1)^*$	3708764	3709200	0.012	3709150	0.010	3709342	0.016
4		$^3P^o\ 0(1)^*$	3744703	3745238	0.014	3745200	0.013	3745145	0.012
5	$2s^22p^53p$	$^1P^o\ 1(2)^*$	3752993	3753600	0.016	3753600	0.016	3753506	0.014
6		$^3S\ 1(1)$	3879300	3879444	0.004	3879370	0.002	3879599	0.008
7		$^3P\ 0(2)$	3949632	3949910	0.007	3949860	0.006	3949877	0.006
8		$^3D\ 2(1)$	3905811	3906203	0.010	3906140	0.008	3906330	0.013
9		$^3D\ 3(1)$	3908590	3908849	0.007	3908820	0.006	3909024	0.011
10		$^3D\ 1(2)$	3917721	3918095	0.010	3918050	0.008	3918218	0.013
11		$^1D\ 2(2)$	3926517	3926887	0.009	3926850	0.008	3927043	0.013
12		$^1P\ 1(3)$	3950645	3951159	0.013	3951160	0.013	3951066	0.011
13		$^3P\ 2(3)$	3964899	3965425	0.013	3965450	0.014	3965329	0.011
14		$^3P\ 1(4)$	3964413	3964847	0.011	3964850	0.011	3964753	0.009
15	$2s^22p^53d$	$^1S\ 0(3)$	4057766	4060030	0.056	4063200	0.134	4060054	0.056
16		$^3P^o\ 0(2)^*$	4163608	4163874	0.006	4163800	0.005	4164048	0.011
17		$^3P^o\ 1(3)^*$	4168003	4168326	0.008	4168240	0.006	4168476	0.011
18		$^3P^o\ 2(2)^*$	4176754	4177038	0.007	4177080	0.008	4177197	0.011
19		$^3D^o\ 1(4)^*$	4220684	4219800	0.021	4219800	0.021	4221203	0.012
20		$^3F^o\ 4(1)^*$	4179158	4179462	0.007	4179420	0.006	4179642	0.012
21		$^3F^o\ 3(1)^*$	4184091	4184514	0.010	4184430	0.008	4184637	0.013
22		$^3F^o\ 2(3)^*$	4193529	4193932	0.010	4193940	0.010	4194059	0.013
23		$^1F^o\ 3(2)^*$	4199249	4199685	0.010	4199650	0.010	4199830	0.014
24		$^1D^o\ 2(4)^*$	4232431	4233020	0.014	4233000	0.013	4232924	0.012
25		$^1D^o\ 3(3)^*$	4238261	4238843	0.014	4238840	0.014	4238749	0.012
26		$^1D^o\ 2(5)^*$	4236893	4237394	0.012	4237450	0.013	4237300	0.010
27	$2s2p^63s$	$^1P^o\ 1(5)^*$	4281869	4281600	0.006	4281600	0.006	4283082	0.028
28		$^3S\ 1(5)$	4529230	4530260	0.023	4530260	0.023	-	-
29		$^1S\ 0(4)$	4565196	-	-	4569000	0.083	-	-
30	$2s2p^63p$	$^3P^o\ 0(3)^*$	4731107	4731780	0.014	4731780	0.014	-	-
31		$^3P^o\ 2(6)^*$	4740622	4741030	0.009	4741030	0.009	-	-
32		$^3P^o\ 1(6)^*$	4733142	4733300	0.003	4733300	0.003	-	-
33		$^1P^o\ 1(7)^*$	4753608	4754000	0.008	4754000	0.008	-	-
34	$2s2p^63d$	$^3D\ 1(6)$	5001722	5003600	0.038	5003600	0.038	-	-
35		$^3D\ 2(4)$	5002107	5004030	0.038	5004030	0.038	-	-
36		$^3D\ 3(2)$	5002854	5004740	0.038	5004740	0.038	-	-
37		$^1D\ 2(5)$	5029742	5009000	0.414	5009000	0.412	-	-

**Table 2.** Wavelengths and branch fractions of E1 decays of levels arising from the  $2s^22p^53l$  and  $2s2p^63l$  configurations in Ti XIII. Only lines of at least 2% branch fraction are listed, for  $\lambda < 130 \text{ \AA}$ .  $J(\#\Pi)$  denotes total angular momentum  $J$ , sequence number  $\#$ , and parity (\* for odd parity).

Wavelength $\lambda(\text{\AA})$	Upper level $J(\#\Pi)$	Lifetime $\tau(s)$	Lower level $J(\#\Pi)$	Branch fraction
21.037	1( 7)*	7.33E-13	0( 1)	0.92
21.128	1( 6)*	5.78E-12	0( 1)	0.44
23.354	1( 5)*	8.90E-14	0( 1)	1.00
23.693	1( 4)*	8.51E-13	0( 1)	0.99
23.992	1( 3)*	2.51E-11	0( 1)	0.78
26.645	1( 2)*	2.37E-12	0( 1)	1.00
26.963	1( 1)*	2.99E-12	0( 1)	1.00
116.10	2( 6)*	1.03E-11	1( 1)	0.03
116.76	0( 4)	1.37E-11	1( 1)*	0.49
117.12	1( 6)*	5.78E-12	1( 1)	0.06
117.24	2( 5)	1.04E-11	2( 2)*	0.02
117.40	0( 3)*	1.03E-11	1( 1)	0.24
118.25	2( 5)	1.04E-11	3( 1)*	0.13
119.32	1( 6)	1.08E-11	0( 2)*	0.07
119.59	2( 5)	1.04E-11	2( 3)*	0.10
119.89	2( 4)	1.08E-11	1( 3)*	0.06
119.94	1( 6)	1.08E-11	1( 3)*	0.11
120.19	2( 6)*	1.03E-11	3( 1)	0.51
120.27	1( 5)	9.75E-12	2( 1)*	0.58
120.41	2( 5)	1.04E-11	3( 2)*	0.22
120.87	1( 6)*	5.78E-12	2( 1)	0.29
120.91	1( 7)*	7.33E-13	2( 2)	0.02
121.05	3( 2)	1.47E-11	2( 2)*	0.08
121.16	2( 4)	1.08E-11	2( 2)*	0.10
121.40	3( 2)	1.47E-11	4( 1)*	0.69
121.88	1( 5)	9.75E-12	1( 1)*	0.19
122.25	2( 4)	1.08E-11	3( 1)*	0.41
122.83	2( 6)*	1.03E-11	2( 2)	0.14
122.94	0( 3)*	1.03E-11	1( 2)	0.47
123.12	0( 4)	1.37E-11	1( 2)*	0.50
123.73	1( 6)	1.08E-11	2( 3)*	0.38
123.97	1( 6)*	5.78E-12	2( 2)	0.03
124.56	2( 4)	1.08E-11	3( 2)*	0.06
125.42	2( 5)	1.04E-11	2( 4)*	0.08
126.13	2( 5)	1.04E-11	2( 5)*	0.08
126.35	2( 5)	1.04E-11	3( 3)*	0.18
127.47	1( 5)	9.75E-12	0( 1)*	0.10
127.63	1( 6)*	5.78E-12	0( 2)	0.04
127.80	1( 6)*	5.78E-12	1( 3)	0.09
127.97	2( 4)	1.08E-11	1( 4)*	0.05
128.04	1( 6)	1.08E-11	1( 4)*	0.14
128.13	0( 3)*	1.03E-11	1( 3)	0.20
128.83	1( 5)	9.75E-12	1( 2)*	0.13
128.83	2( 6)*	1.03E-11	1( 4)	0.08
128.91	2( 6)*	1.03E-11	2( 3)	0.15
129.93	2( 4)	1.08E-11	2( 4)*	0.11
129.99	1( 6)	1.08E-11	2( 4)*	0.15

**Table 3.** Wavelengths and branch fractions of E1 decays of levels arising from the  $2s^2 2p^5 3l$  and  $2s 2p^6 3l$  configurations in Ti XIII. Only lines of at least 2% branch fraction are listed, for  $\lambda > 130 \text{ \AA}$ .  $J(\#)\Pi$  denotes total angular momentum  $J$ , sequence number  $\#$ , and parity (\* for odd parity).

Wavelength $\lambda(\text{\AA})$	Upper level $J(\#)\Pi$	Lifetime $\tau(s)$	Lower level $J(\#)\Pi$	Branch fraction
130.43	0( 3)*	1.03E-11	1( 4)	0.05
130.56	3( 2)	1.47E-11	2( 5)*	0.08
130.68	2( 4)	1.08E-11	2( 5)*	0.06
130.92	2( 4)	1.08E-11	3( 3)*	0.04
133.71	2( 5)	1.04E-11	1( 5)*	0.07
286.53	0( 3)	6.09E-11	1( 1)*	0.42
328.11	0( 3)	6.09E-11	1( 2)*	0.58
336.19	2( 2)*	1.15E-10	1( 1)	0.54
344.05	3( 2)*	1.06E-10	3( 1)	0.21
346.38	1( 3)*	2.51E-11	1( 1)	0.17
347.56	2( 3)*	1.02E-10	2( 1)	0.36
351.73	0( 2)*	1.14E-10	1( 1)	0.91
354.88	2( 4)*	1.02E-10	1( 3)	0.86
359.35	3( 1)*	1.07E-10	2( 1)	0.84
362.14	2( 5)	1.04E-11	1( 7)*	0.10
362.57	2( 3)*	1.02E-10	1( 2)	0.61
362.98	3( 1)*	1.07E-10	3( 1)	0.15
365.82	3( 3)*	1.09E-10	2( 3)	0.97
366.66	3( 2)*	1.06E-10	2( 2)	0.78
367.00	2( 5)*	1.04E-10	1( 4)	0.76
369.53	1( 6)	1.08E-11	0( 3)*	0.06
369.59	4( 1)*	1.14E-10	3( 1)	1.00
371.80	2( 4)	1.08E-11	1( 6)*	0.07
372.33	1( 6)	1.08E-11	1( 6)*	0.04
375.06	1( 4)	2.08E-10	2( 1)*	0.15
381.34	3( 2)	1.47E-11	2( 6)*	0.13
399.62	2( 2)*	1.15E-10	2( 2)	0.30
415.17	0( 2)	1.84E-10	1( 1)*	0.81
437.20	2( 2)	2.01E-10	2( 1)*	0.59
455.15	1( 4)	2.08E-10	0( 1)*	0.48
459.24	2( 2)	2.01E-10	1( 1)*	0.40
471.91	2( 3)	2.28E-10	1( 2)*	0.93
472.99	1( 4)	2.08E-10	1( 2)*	0.37
473.06	2( 6)*	1.03E-11	1( 5)	0.05
474.38	3( 1)	2.42E-10	2( 1)*	1.00
478.57	1( 2)	2.48E-10	1( 1)*	0.87
480.72	2( 1)	2.75E-10	2( 1)*	0.49
485.57	1( 3)	2.79E-10	0( 1)*	0.49
490.41	1( 6)*	5.78E-12	1( 5)	0.02
495.35	0( 3)*	1.03E-11	1( 5)	0.04
505.94	1( 3)	2.79E-10	1( 2)*	0.49
507.49	2( 1)	2.75E-10	1( 1)*	0.51
508.55	0( 2)	1.84E-10	1( 2)*	0.19
550.93	1( 1)	4.37E-10	2( 1)*	0.88

**Table 4.** Level energies of  $2s^22p^53l$  and  $2s2p^63l$  levels in Ca XI. Comparison of the results of our calculations with NIST on-line data basis. Deviations (in percent) relate to our calculations.

Index	Configuration	Term	$J$	Energy ( $\text{cm}^{-1}$ )		
				NIST	This work	Deviation
1	$2s^22p^6$	$^1S$	0	0	0	-
2	$2s^22p^53s$	$^3P^o$	2	-	2801819	-
3		$^3P^o$	1	2810900	2810588	0.011
4	$2s^22p^53p$	$^3P^o$	0	-	2831670	-
5		$^1P^o$	1	2839900	2839386	0.018
6		$^3S$	1	-	2953594	-
7		$^3D$	2	-	2977968	-
8		$^3D$	3	-	2978276	-
9		$^1P$	1	-	2986513	-
10		$^3P$	2	-	2993336	-
11		$^3D$	1	-	3006932	-
12		$^3P$	0	-	3009000	-
13		$^1D$	2	-	3016378	-
14	$^3D$	1	-	3016845	-	
15	$2s^22p^53d$	$^1S$	0	-	3098308	-
16		$^3P^o$	0	-	3195830	-
17		$^3P^o$	1	3199300	3198902	0.012
18		$^3P^o$	2	-	3205169	-
19		$^3F^o$	4	-	3208165	-
20		$^3F^o$	3	-	3212144	-
21		$^1D^o$	2	-	3219428	-
22		$^3D^o$	3	-	3224078	-
23		$^3D^o$	1	3239700	3239308	0.012
24		$^3F^o$	2	-	3244161	-
25	$^3D^o$	2	-	3247805	-	
26	$^1F^o$	3	-	3248099	-	
27	$^1P^o$	1	3284300	3283473	0.025	
28	$2s2p^63s$	$^3S$	1	-	3520024	-
29		$^1S$	0	-	3550218	-
30	$2s2p^63p$	$^3P^o$	0	-	3691165	-
31		$^3P^o$	1	3692900	3692521	-
32		$^3P^o$	2	-	3696835	-
33	$2s2p^63d$	$^1P^o$	1	3708900	3708424	0.013
34		$^3D$	1	-	3917893	-
35		$^3D$	2	-	3918054	-
36		$^3D$	3	-	3918399	-
37		$^1D$	2	-	3939621	-

**Table 5.** Level energies of  $2s^22p^53l$  and  $2s2p^63l$  levels in Sc XII. Comparison of the results of our calculations with NIST on-line data basis. Deviations (in percent) relate to our calculations.

Index	Configuration	Term	$J$	Energy ( $cm^{-1}$ )			
				NIST	This work	Deviation	
1	$2s^22p^6$	$^1S$	0	0	0	-	
2	$2s^22p^53s$	$^3P^o$	2	3235171	3234779	0.012	
3		$^3P^o$	1	3245100	3244655	0.014	
4		$^3P^o$	0	3272730	3272438	0.009	
5		$^1P^o$	1	3280800	3280437	0.011	
6		$2s^22p^53p$	$^3S$	1	3401413	3401296	0.003
7			$^3D$	2	3427225	3426862	0.011
8			$^3D$	3	3428533	3428224	0.009
9			$^3D$	1	3437344	3436986	0.010
10			$^1D$	2	3445090	3444716	0.011
11			$^1P$	1	3463292	3463034	0.007
12			$^3P$	0	3464198	3463856	0.010
13			$^3P$	2	3474958	3474706	0.007
14			$^3P$	1	3474958	3474733	0.006
15			$2s^22p^53d$	$^1S$	0	3564763	3562528
16	$^3P^o$	0		-	3664559	-	
17	$^3P^o$	1		3668546	3668262	0.008	
18	$^3P^o$	2		3675982	3675727	0.007	
19	$^3F^o$	4		3678797	3678472	0.009	
20	$^3F^o$	3		3683330	3682954	0.010	
21	$^1D^o$	2		3691702	3691309	0.011	
22	$^3D^o$	3		3696911	3696475	0.012	
23	$^3D^o$	1		3714700	3714636	0.002	
24	$^3F^o$	2		3722705	3722429	0.007	
25	$^3D^o$	2		3726769	3726480	0.008	
26	$^1F^o$	3		3727574	3727272	0.008	
27	$2s2p^63s$	$^1P^o$	1	3767300	3766943	0.009	
28		$^3S$	1	-	4008805	-	
29	$2s2p^63p$	$^1S$	0	-	4041863	-	
30		$^3P^o$	0	-	4195304	-	
31		$^3P^o$	1	4198000	4196985	0.024	
32		$^3P^o$	2	-	4202717	-	
33		$^1P^o$	1	4215000	4215014	0.000	
34		$2s2p^63d$	$^3D$	1	-	4443958	-
35			$^3D$	2	-	4444226	-
36	$^3D$		3	-	4444760	-	
37	$^1D$		2	-	4468776	-	

**Table 6.** Level energies of  $2s^22p^53l$  and  $2s2p^63l$  levels in VXIV. Comparison of the results of our calculations with NIST on-line data basis. Deviations (in percent) relate to our calculations.

Index	Configuration	Term	$J$	Energy (cm <sup>-1</sup> )		
				NIST	This work	Deviation
1	$2s^22p^6$	$^1S$	0	0	0	-
2	$2s^22p^53s$	$^3P^o$	2	4190606	4190757	0.004
3		$^3P^o$	1	4202700	4202818	0.003
4	$2s^22p^53p$	$^3P^o$	0	4248410	4248544	0.003
5		$^1P^o$	1	4257100	4257132	0.001
6		$^3S$	1	4387211	4387542	0.008
7		$^3D$	2	4414607	4414759	0.003
8		$^3D$	3	4419174	4419366	0.004
9		$^1P$	1	4428554	4428708	0.003
10		$^3P$	2	4438597	4438727	0.003
11		$^3P$	0	4466070	4466336	0.006
12		$^3D$	1	4469715	4469874	0.004
13		$^3P$	1	4485944	4486060	0.003
14	$^1D$	2	4487045	4487120	0.002	
15	$2s^22p^53d$	$^1S$	0	4585819	4584105	0.037
16		$^3P^o$	0	4692510	4693010	0.011
17		$^3P^o$	1	4696000	4698155	0.046
18		$^3P^o$	2	4708057	4708272	0.005
19		$^3F^o$	4	4710105	4710265	0.003
20		$^3F^o$	3	4715469	4715581	0.002
21		$^1D^o$	2	4726016	4726110	0.002
22		$^3D^o$	3	4732377	4732442	0.001
23		$^3D^o$	1	4757800	4757480	0.007
24		$^3F^o$	2	4774275	4774380	0.002
25		$^3D^o$	2	4779239	4779274	0.001
26		$^1F^o$	3	4781291	4781284	0.000
27		$^1P^o$	1	4827200	4828432	0.026
28	$2s2p^63s$	$^3S$	1	-	5081401	-
29		$^1S$	0	-	5120311	-
30	$2s2p^63p$	$^3P^o$	0	-	5298711	-
31		$^3P^o$	1	5299000	5301125	0.040
32		$^3P^o$	2	-	5310731	-
33	$2s2p^63d$	$^1P^o$	1	5324000	5324386	0.007
34		$^3D$	1	-	5591537	-
35		$^3D$	2	-	5592063	-
36		$^3D$	3	-	5593069	-
37		$^1D$	2	-	5622847	-

**Table 7.** Level energies of  $2s^22p^53l$  and  $2s2p^63l$  levels in Cr XV. Comparison of the results of our calculations with NIST on-line data basis. Deviations (in percent) relate to our calculations.

Index	Configuration	Term	$J$	Energy (cm <sup>-1</sup> )		
				NIST	This work	Deviation
1	$2s^22p^6$	$^1S$	0	0	0	-
2	$2s^22p^53s$	$^3P^o$	2	4714294	4713622	0.014
3		$^3P^o$	1	4727500	4726754	0.016
4	$2s^22p^53p$	$^3P^o$	0	4784174	4784081	0.002
5		$^1P^o$	1	4793200	4792975	0.005
6		$^3S$	1	4926429	4925978	0.009
7		$^3D$	2	4954368	4953672	0.014
8		$^3D$	3	4961187	4960573	0.012
9		$^1P$	1	4970636	4969969	0.013
10		$^3P$	2	4982062	4981365	0.014
11		$^3P$	0	5014563	5013994	0.011
12		$^3D$	1	5020941	5020870	0.001
13		$^3P$	1	5039971	5039892	0.002
14	$2s^22p^53d$	$^1D$	2	5041714	5041570	0.003
15		$^1S$	0	5143616	5141673	0.038
16		$^3P^o$	0	5253448	5252800	0.012
17		$^3P^o$	1	5259419	5258748	0.013
18		$^3P^o$	2	5270945	5270306	0.012
19		$^3F^o$	4	5272468	5271839	0.012
20		$^3F^o$	3	5278128	5277452	0.013
21		$^1D^o$	2	5289794	5289082	0.013
22		$^3D^o$	3	5296812	5296098	0.013
23		$^3D^o$	1	5324200	5325046	0.016
24		$^3F^o$	2	5348574	5348497	0.001
25		$^3D^o$	2	5354045	5353871	0.003
26		$^1F^o$	3	5356770	5356571	0.004
27		$^1P^o$	1	5406300	5406858	0.010
28	$2s2p^63s$	$^3S$	1	-	5665452	-
29		$^1S$	0	5749300	5707335	0.730
30	$2s2p^63p$	$^3P^o$	0	-	5898284	-
31		$^3P^o$	1	5894500	5901096	0.112
32		$^3P^o$	2	-	5913264	-
33	$2s2p^63d$	$^1P^o$	1	5921000	5927567	0.111
34		$^3D$	1	-	6213686	-
35		$^3D$	2	-	6214382	-
36		$^3D$	3	-	6215707	-
37		$^1D$	2	-	6248368	-

**Table 8.** Level energies of  $2s^22p^53l$  and  $2s2p^63l$  levels in Mn XVI. Comparison of the results of our calculations with NIST on-line data basis. Deviations (in percent) relate to our calculations.

Index	Configuration	Term	$J$	Energy (cm <sup>-1</sup> )			
				NIST	This work	Deviation	
1	$2s^22p^6$	$^1S$	0	0	0	-	
2	$2s^22p^53s$	$^3P^o$	2	5266964	5266359	0.011	
3		$^3P^o$	1	5281200	5280548	0.012	
4		$^3P^o$	0	5351520	5351482	0.001	
5		$^1P^o$	1	5360800	5360689	0.002	
6		$2s^22p^53p$	$^3S$	1	5494974	5494564	0.007
7			$^3D$	2	5523101	5522529	0.010
8			$^3D$	3	5532778	5532242	0.010
9			$^1P$	1	5542158	5541545	0.011
10			$^3P$	2	5555050	5554464	0.011
11			$^3P^o$	0	-	5592639	-
12	$^3D$		1	5603789	5603800	0.000	
13	$^3P$		1	5626306	5626144	0.003	
14	$^1D$		2	5628520	5628475	0.001	
15	$2s^22p^53d$		$^1S$	0	-	5730650	-
16		$^3P^o$	0	5843409	5843008	0.007	
17		$^3P^o$	1	5850249	5849811	0.007	
18		$^3P^o$	2	5863347	5862883	0.008	
19		$^3F^o$	4	5864439	5863926	0.009	
20		$^3F^o$	3	5870337	5869731	0.010	
21		$^1D^o$	2	5883137	5882478	0.011	
22		$^3D^o$	3	5890952	5890266	0.012	
23		$^3D^o$	1	5923500	5923398	0.002	
24		$^3F^o$	2	-	5955010	-	
25	$^3D^o$	2	5961148	5960939	0.004		
26	$^1F^o$	3	5964431	5964364	0.001		
27	$2s2p^63s$	$^1P^o$	1	6018300	6017384	0.015	
28		$^3S$	1	-	6281571	-	
29		$^1S$	0	-	6326448	-	
30	$2s2p^63p$	$^3P^o$	0	-	6530017	-	
31		$^3P^o$	1	6530800	6533243	0.037	
32		$^3P^o$	2	-	6548467	-	
33	$2s2p^63d$	$^1P^o$	1	6562500	6563400	0.014	
34		$^3D$	1	-	6868436	-	
35		$^3D$	2	-	6869336	-	
36		$^3D$	3	-	6871053	-	
37		$^1D$	2	-	6906573	-	

**Table 9.** Level energies of  $2s^22p^53l$  and  $2s2p^63l$  levels in Fe XVII. Comparison of the results of our calculations with NIST on-line data basis. Deviations (in percent) relate to our calculations.

Index	Configuration	Term	$J$	Energy (cm <sup>-1</sup> )		
				NIST	This work	Deviation
1	$2s^22p^6$	$^1S$	0	0	0	-
2	$2s^22p^53s$	$^3P^o$	2	5849491	5848891	0.010
3		$^3P^o$	1	5864771	5864138	0.011
4	$2s^22p^53p$	$^3P^o$	0	5951211	5950877	0.006
5		$^1P^o$	1	5960870	5960410	0.008
6		$^3S$	1	6093451	6093209	0.004
7		$^3D$	2	6121691	6121253	0.007
8		$^3D$	3	6134730	6134360	0.006
9		$^1P$	1	6143851	6143431	0.007
10		$^3P$	2	6158470	6158010	0.007
11		$^3P$	0	6202250	6202238	0.000
12		$^3D$	1	6219030	6218795	0.004
13		$^3P$	1	6245210	6245018	0.003
14	$2s^22p^53d$	$^1D$	2	6248261	6248024	0.004
15		$^1S$	0	6353410	6351136	0.036
16		$^3P^o$	0	6463980	6463611	0.006
17		$^3P^o$	1	6471801	6471317	0.007
18		$^3P^o$	2	6486401	6485977	0.007
19		$^3F^o$	4	6486831	6486514	0.005
20		$^3F^o$	3	6493031	6492387	0.010
21		$^1D^o$	2	6506700	6506276	0.007
22		$^3D^o$	3	6515350	6514936	0.006
23		$^3D^o$	1	6552200	6552491	0.004
24		$^3F^o$	2	6594361	6594099	0.004
25		$^3D^o$	2	6600950	6600688	0.004
26		$^1F^o$	3	6605151	6604858	0.004
27		$^1P^o$	1	6660000	6660232	0.003
28	$2s2p^63s$	$^3S$	1	-	6929964	-
29		$^1S$	0	7010001	6977876	0.458
30	$2s2p^63p$	$^3P^o$	0	-	7194137	-
31		$^3P^o$	1	7198901	7197788	0.015
32		$^3P^o$	2	-	7216629	-
33	$2s2p^63d$	$^1P^o$	1	7234300	7232164	0.030
34		$^3D$	1	-	7556104	-
35		$^3D$	2	-	7557249	-
36		$^3D$	3	-	7559441	-
37		$^1D$	2	-	7597767	-

**Table 10.** Wavelengths and branch fractions of E1 decays of levels arising from the  $2s^2 2p^5 3l$  and  $2s 2p^6 3l$  configurations in Ca XI, together with lines observed after foil excitation of Ca ion beams of 8 and 11 MeV that are close in wavelength. oor indicates line positions out of range of the spectra recorded. Only lines of at least 3% predicted branch fraction are listed, for  $\lambda > 340 \text{ \AA}$ .  $J(\#)\Pi$  denotes total angular momentum  $J$ , sequence number  $\#$ , and parity (\* for odd parity).

Observed		Calculated			
Wavelength	Wavelength	Upper level	Lifetime	Lower level	Branch
$\lambda(\text{\AA})$	$\lambda(\text{\AA})$	$J(\#)\Pi$	$\tau(s)$	$J(\#)\Pi$	fraction
oor	347.56	0(3)	7.94E-11	1(1)*	0.35
385.7	386.22	0(3)	7.94E-11	1(2)*	0.65
-	392.98	2(5)*	1.24E-10	2(2)	0.10
397.0	397.50	2(2)*	1.37E-10	1(1)	0.56
406.6	406.83	3(2)*	1.27E-10	3(1)	0.20
407.6	407.65	1(3)*	4.51E-11	1(1)	0.26
412.9	412.82	0(2)*	1.36E-10	1(1)	0.87
414.3	414.15	2(3)*	1.24E-10	2(1)	0.35
421.5	421.53	2(4)*	1.22E-10	1(3)	0.85
427.1	427.03	3(1)*	1.29E-10	2(1)	0.84
427.3	427.59	3(1)*	1.29E-10	3(1)	0.15
429.3	429.34	2(3)*	1.24E-10	1(2)	0.63
431.5	431.55	3(3)*	1.28E-10	2(3)	0.96
-	432.10	2(5)*	1.24E-10	2(3)	0.09
-	432.53	2(5)	1.27E-11	1(7)*	0.10
433.0	432.98	2(5)*	1.24E-10	1(4)	0.74
433.4	433.38	3(2)*	1.27E-10	2(2)	0.78
435.0	434.99	4(1)*	1.35E-10	3(1)	1.00
439.0	439.01	2(4)*	1.22E-10	2(3)	0.10
441.0	441.06	1(6)	1.31E-11	0(3)*	0.05
-	443.39	2(4)	1.30E-11	1(6)*	0.07
443.8	443.71	1(6)	1.31E-11	1(6)*	0.04
-	451.34	3(2)	1.30E-11	2(6)*	0.09
464.9	465.06	1(4)	2.65E-10	2(1)*	0.18
471.4	472.07	2(2)*	1.37E-10	2(2)	0.29
503.4	504.00	0(2)	2.39E-10	1(1)*	0.81
522.2	522.15	2(2)	2.61E-10	2(1)*	0.59
539.6	540.03	1(4)	2.65E-10	0(1)*	0.43
542.2	541.44	1(2)	3.15E-10	2(1)*	0.14
547.2	547.20	2(2)	2.61E-10	1(1)*	0.37
bl	558.71	0(2)*	1.36E-10	1(4)	0.05
564.4	563.51	1(4)	2.65E-10	1(2)*	0.39
564.4	565.00	2(3)	2.92E-10	1(2)*	0.89
565.4	565.58	2(6)*	1.24E-11	1(5)	0.04
567.0	566.71	3(1)	3.12E-10	2(1)*	1.00
567.0	567.70	2(1)	3.41E-10	2(1)*	0.47
568.7	568.42	1(2)	3.15E-10	1(1)*	0.83
570.7	570.57	1(3)	3.41E-10	0(1)*	0.52
-	579.72	1(6)*	9.42E-12	1(5)	0.03
-	584.31	0(3)*	1.25E-11	1(5)	0.04
589.6	589.57	0(2)	2.39E-10	1(2)*	0.19
596.8	596.85	1(3)	3.41E-10	1(2)*	0.46
597.5	597.44	2(1)	3.41E-10	1(1)*	0.53
oor	658.87	1(1)	5.64E-10	2(1)*	0.84
oor	699.27	1(1)	5.64E-10	1(1)*	0.13

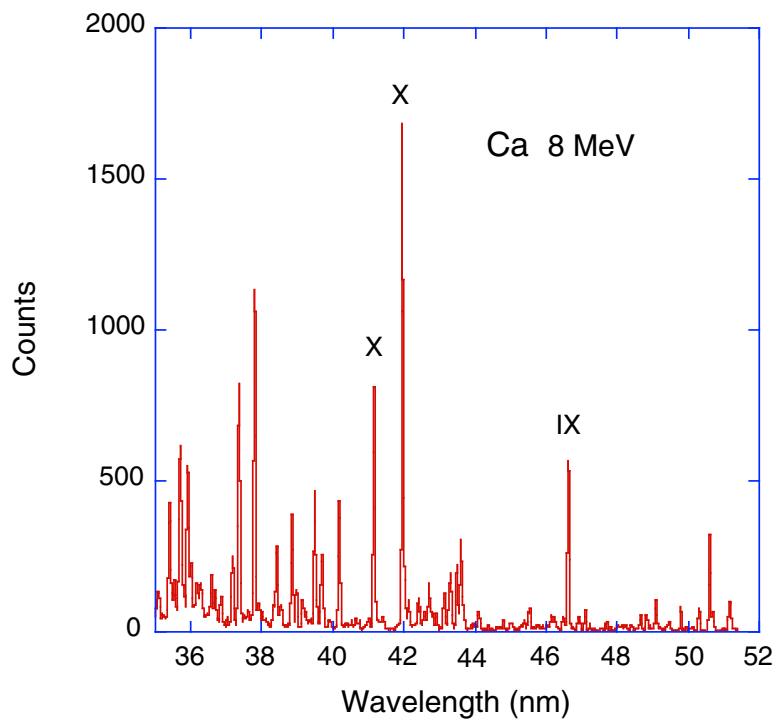


**Figure 1.** Section of the EUV spectrum of foil-excited calcium. The dominant contributions are from Na-like Ca X  $3p - 3d$  and Ca IX  $3s^2 - 3s3p$  transitions. Of Ne-like Ca XI, about 15, individually weaker, lines are expected to show (see table 10).